Journal of Polymer Science

WILEY

JOURNAL OF POLYMER SCIENCE

RESEARCH ARTICLE OPEN ACCESS

Do Nucleating Agents or Processing Methods Affect the Thermal Transport in RacoPP?

Ina Klein[1] | María Ester Marroquin Lacayo[1] | Thomas Blesch[2] | Sabine Rosenfeldt[1] | Patrick Länger[3] | Klaus Kreger[2] | Stefan Rettinger[1] | Jürgen Senker[3,4,5] | Hans-Werner Schmidt[2,4] | Markus Retsch[1,4,5]

[1]Department of Chemistry, Physical Chemistry I, University of Bayreuth, Bayreuth, Germany | [2]Department of Chemistry, Macromolecular Chemistry I, University of Bayreuth, Bayreuth, Germany | [3]Department of Chemistry, Inorganic Chemistry III, University of Bayreuth, Bayreuth, Germany | [4]Bavarian Polymer Institute (BPI), Bayreuth Center for Colloids and Interfaces, University of Bayreuth, Bayreuth, Germany | [5]Bavarian Center for Battery Technology (BayBatt), University of Bayreuth, Bayreuth, Germany

Correspondence: Markus Retsch (markus.retsch@uni-bayreuth.de)

Received: 19 November 2024 | **Revised:** 27 January 2025 | **Accepted:** 30 January 2025

Funding: This work was supported by Collaborative Research Centre 1585, Projects A04 and C05 of the German Research Foundation (grant number: 492723217).

Keywords: compression molding | injection molding | nucleating agent | polypropylene | thermal transport

ABSTRACT

Polypropylene (PP) homopolymers and copolymers play a pivotal role in the plastics industry. With applications spanning automotive components, electronic housings, construction materials, and food packaging, understanding their thermal transport properties is essential. This study investigates the impact of a highly efficient 1,3,5-benzenetrisamide (BTA) nucleator (N,N′,N″-tris(3-methylbutyl)benzene-1,3,5-tricarboxamide) on the thermal diffusivity of injection- and compression-molded propylene-ethylene random copolymer (racoPP). Results are compared with those for a less efficient BTA (N,N′,N″-tris(n-butyl) benzene-1,3,5-tricarboxamide) and a control sample without additives. We supplement our thermal characterizations with x-ray diffraction (XRD) and small-angle x-ray scattering (SAXS) analyses and demonstrate that the processing method and the presence of BTAs can impact the crystallinity and orientation of the PP lamellae. However, the thermal diffusivity of racoPP exhibits remarkable resilience to these changes, ensuring the consistent performance that is often required in industrial applications.

1 | Introduction

Polypropylene (PP) is one of the most widely applied plastics worldwide [1]. It shows low density, great mechanical properties, and thermal resistance at low costs. These properties strongly depend on the microstructure and morphology of the PP object, which can be controlled by the processing parameters and by the addition of suitable additives and fillers [1, 2]. Controlling and promoting the nucleation in PP and in related copolymers is used to reduce the cycle time during processing and to improve its mechanical and optical properties [3]. This includes the increase of flexural strength and modulus, tensile strength and modulus, impact resistance, rigidity, clarity, reduction of haze, and even the enhancement of charge-storage properties [4–9]. Injection molding represents one of the most applied industrial manufacturing methods for PP. The polymer is heated until melting and injected into a cold mold, where it solidifies into the shape of the mold [1, 10]. Thereby, the process parameters, such as temperature, shear force, cooling rate, and pressure, all affect the properties of the obtained PP product. Owing to the semicrystalline nature of iso-tactic PP (iPP), this includes the ratio of the crystal modifications (α, β, γ), the ratio of the amorphous to crystalline phase, the presence and size of three-dimensional spherulites, oriented lamellar crystallites, shish-kebab structures, and gradients and blends of such morphologies [2, 10–14]. Due to these numerous levers affecting the polymer's microstructure and thereby its properties, many papers address injection-molded

PP and, thereby, add another important aspect to the complex topic [8, 11, 13, 15–19]. Particularly, the temperature evolution upon cooling an iPP melt is critical for the crystal nucleation and crystal growth rate and, therefore, decisive for the crystallite microstructure [2, 10, 11]. Increasing the cooling rate, for instance via thermally conductive fillers, can significantly increase the number of nucleation sites [2, 10]. A similar effect can be achieved by adding nucleating agents to the polymer melt. The nucleators raise the crystallization temperature and accelerate crystal nucleation by providing numerous heterogeneous nucleation sites in the melt. This leads to smaller spherulite sizes [5–7, 19]. In addition to the nucleation via heterogeneous additives, shear can induce orientation-induced primary iPP nuclei. They lead to accelerated crystallization and oriented lamellar structures (kebab structures) perpendicular to the flow direction. Note that the primary nuclei may be long fibrillar extended chain crystals (shish structures), but they may also be small clusters of aligned chains. Hence, the evolution of shish structures is not necessary for the formation of oriented kebab structures. Furthermore, the extent of crystal orientation is dependent on factors such as the molecular weight distribution, the strain, and the shear rate [12].

1,3,5-Benzenetrisamide (BTA) derivatives represent an excellent and versatile family of nucleating agents. The good solubility of several BTA types in an iPP melt ensures a homogeneous distribution of the additive. Even at very low weight fractions, these additives can significantly enhance nucleation and induce high transparency and clarity of iPP [4, 7, 20–22]. Furthermore, depending on the chosen BTA, different crystal modifications of iPP can be selectively induced [20, 23]. Here, we focus specifically on their nucleation effect in a propylene-ethylene random copolymer (racoPP). RacoPPs contain a small amount of ethylene as a comonomer and can be regarded as iPP, with the comonomer acting as defects in the polymer chain sequence [24]. As a result, racoPPs have a lower melting point, higher transparency, and improved toughness compared with iPP, while supramolecular nucleating agents, such as distinct BTAs, remain similarly effective [1, 21]. As the polymer melt cools, the BTA molecules crystallize into finely dispersed, highly ordered fibrils. Based on lattice matching, BTA crystals serve as efficient nucleation sites for the racoPP, fostering epitaxial growth [21, 22, 25, 26]. Consequently, BTAs represent a highly interesting additive in various applications, and their influence on the melt temperature, optical, and mechanical properties is intensively studied, along with desired effects. The influence of the PP microstructure on the thermal conductivity of the resulting macroscopic objects has, however, been scarcely studied up to now. The widespread utilization of PP copolymers in electronic housings, automotive components, or food packaging necessitates an understanding of its thermal transport properties. One must be aware that processing, post-processing, and the addition of nucleating agents may impact the thermal transport characteristics. Herein, it is our objective to provide clarity on this matter. We investigate how the presence of N,N′,N″-tris(isopentyl)benzene-1,3,5-tricarboxamide (iPe-BTA), which is known to efficiently nucleate iPP, affects the thermal diffusivity of injection-molded racoPP. It is compared with N,N′,N″-tris(n-butyl)benzene-1,3,5-tricarboxamide (nBu-BTA), a structurally similar BTA additive that has a low nucleation capability, and with no additive at all [20, 21]. The chemical structure of the chosen BTAs is shown in Figure 1a. Moreover, we explore the influence of further processing by pressing the injection-molded samples into thin films and subsequently compare the thermal diffusivities once again. These assessments are supported by structural analyses to unveil the potential presence of an underlying structure–property relationship.

2 | Results and Discussion

2.1 | Injection-Molded Samples

To comprehensively study the influence of the BTAs on the racoPP morphology, a series of injection-molded samples were prepared with a diameter of approximately 27.0 mm and a thickness of about 1.1 mm. Three BTA concentrations were selected: 0.5 wt%, 0.1 wt%, and 0.05 wt%, which ensure a sufficient amount of BTA for the formation of nanofibrils in the racoPP while maintaining good processability for injection-molding. X-ray diffraction (XRD) analysis was performed to assess the impact of the BTAs on the polymer's crystallinity. The results for a concentration of 0.5 wt% are exemplarily shown in Figure 1b. Although the difference in the calculated crystallinities is small, and the absolute values should be interpreted with caution, their comparison follows the expected trend: RacoPP with iPe-BTA exhibits the highest relative crystallinity (46%), followed by racoPP containing nBu-BTA (41%), and finally neat racoPP (38%) (Figure S1). The reflections below 10°, visible for the samples containing nBu-BTA or iPe-BTA, correspond to the most intense reflections of BTA nanocrystallites. They demonstrate that the BTA molecules are self-assembled rather than being molecularly dispersed within the polymer. These supramolecular nano-objects of either BTA type function as nucleation sites in the polymer melt, hereby lowering the energy barrier for the polymer nucleation [21, 22]. The differences between the two types of BTA may be reasoned by a superior nucleation performance of iPe-BTA compared with nBu-BTA. We confirm this by studying the crystallization behavior of racoPP in the presence of the additives, showing a higher crystallization temperature of racoPP with iPe-BTA than with nBu-BTA (Figure S3). It is generally acknowledged that lattice matching is a prerequisite for the nucleation capability of additives; thus, we can attribute the difference in nucleation performance to a better lattice match of iPe-BTA with racoPP than nBu-BTA with racoPP [21, 26].

Small-angle x-ray scattering (SAXS) measurements of injection-molded samples supplement the data on the Ångström range by the nanometer length scale. Figure 1c shows the SAXS patterns of three injection-molded racoPP samples with different concentrations of iPe-BTA. Hereby, we distinguish three sample positions, which were exposed to different shear rates during processing. “top” represents a point in the top-third of the sample that is furthest away from the inlet where the material is injected during processing. “middle” represents the center point of the circular sample and “bottom” is in the center of the bottom-third, closest to the inlet. All samples and all sample positions show a pronounced anisotropy in the SAXS pattern, characterized by broad meridional maxima. During injection-molding the BTAs form thin columnar structures, which are oriented in the direction of the flow. These function as nucleation sites for epitaxial growth of racoPP [22, 25]. As a result, kebab structures with

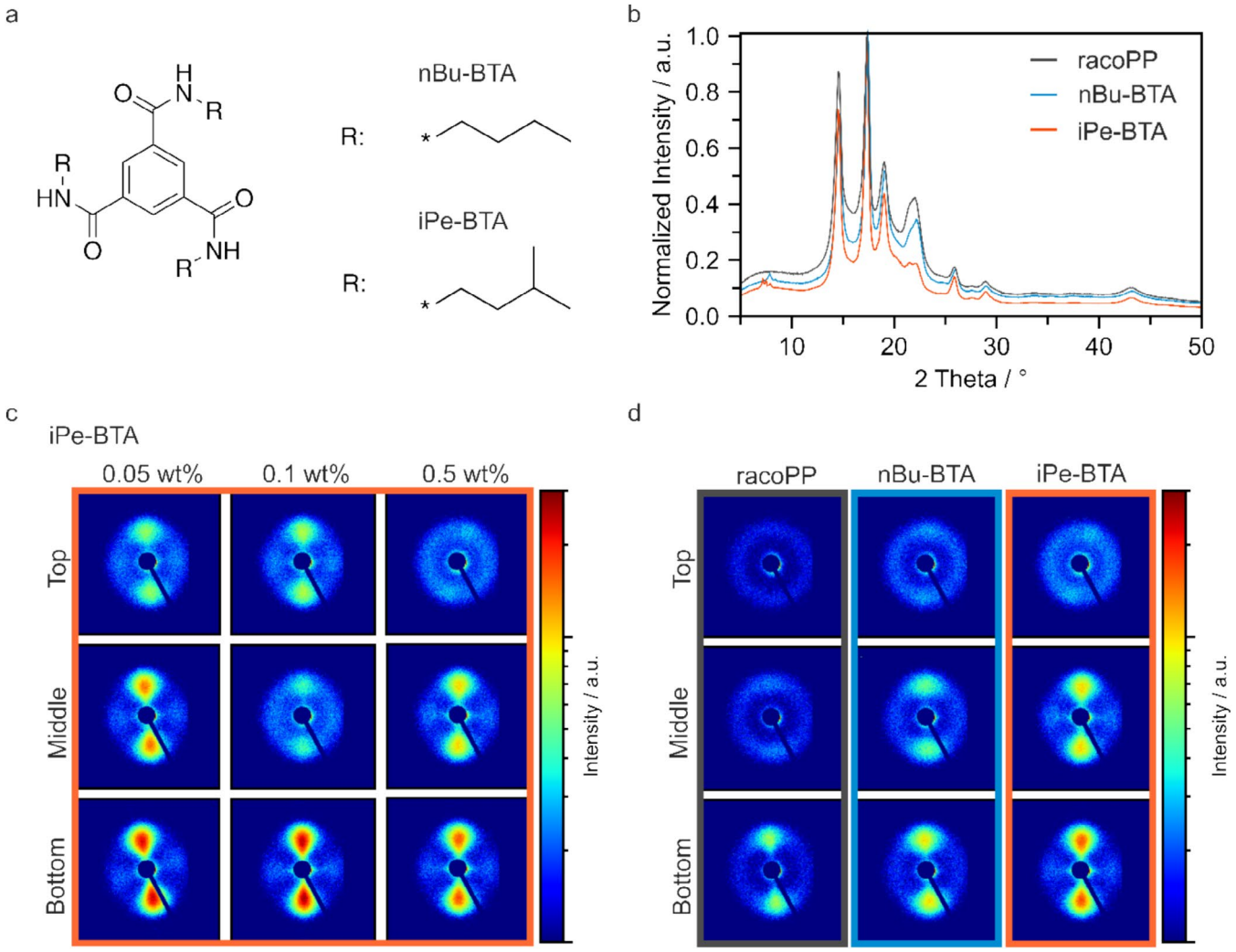

FIGURE 1 | (a) Molecular structure of the utilized nBu-BTA and iPe-BTA. (b) XRD of injection-molded neat racoPP, racoPP with 0.5 wt% nBu-BTA and with 0.5 wt% iPe-BTA. Intensities are normalized to the highest peak. (c) 2D SAXS patterns of injection-molded racoPP with variation in iPe-BTA content and sample position (with "top" furthest from the inlet, "bottom" closest to the inlet and "middle" in between). (d) 2D SAXS patterns of injection-molded neat racoPP, racoPP with 0.5 wt% nBu-BTA and with 0.5 wt% iPe-BTA at different sample positions. The colors are crucial for displaying the results, especially in c and d, to visualize differences in the SAXS patterns. The colors in b and the frames in c and d help to distinguish the sample types.

an orientation perpendicular to the flow direction evolve, which is mirrored in the dumbbell-like intensity distribution of the SAXS patterns. The meridional maxima are most pronounced at positions closest to the inlet for all three concentrations. As the distance increases, their distinctiveness diminishes, giving rise to a more circular intensity distribution. The concentration of 0.1 wt% iPe-BTA initially appears to be an exception, as the top position exhibits a more anisotropic pattern compared with the middle position. However, this initial impression does not hold true. A more detailed examination at various positions across the injection-molded racoPP sample with 0.1 wt% iPe-BTA reveals a general increase in the azimuthal intensity distribution with growing distance from the inlet (Figure S4). Consequently, the deviation observed at the middle position in Figure 1c is likely attributable to a more amorphous region of the sample being probed by the x-ray, which reduces the signal intensity at this specific position and gives the misleading appearance of an outlier. A slightly higher crystallinity at the bottom of the sample (48% for 0.5 wt% iPe-BTA) compared with the top (45% for 0.5 wt% iPe-BTA) implies a higher concentration of orientable lamellar structures near the inlet. More importantly, higher shear flow near the inlet enhances the orientation of the fibrillar nucleation sites. Therefore, with increasing proximity to the inlet, a larger fraction of the existing lamellar crystallites has a preferred orientation. Comparing the different concentrations at the same measurement positions (excluding the apparent outlier) reveals that all samples produce similarly anisotropic patterns. In the case of 0.5 wt%, the absolute scattering intensity is slightly reduced. We do not attribute this observation to the degree of crystallinity, as the values for the samples with 0.05 wt%, 0.1 wt%, and 0.5 wt% iPe-BTA are comparable, at 44%, 46%, and 46%, respectively. Therefore, slight variations in the specimen thickness, the instrumental setting, or the scattering contrast might be the reason for the reduced scattering intensity at 0.5 wt%.

In Figure 1d the patterns of neat racoPP are compared with those containing 0.5 wt% BTA. The results for neat racoPP show that

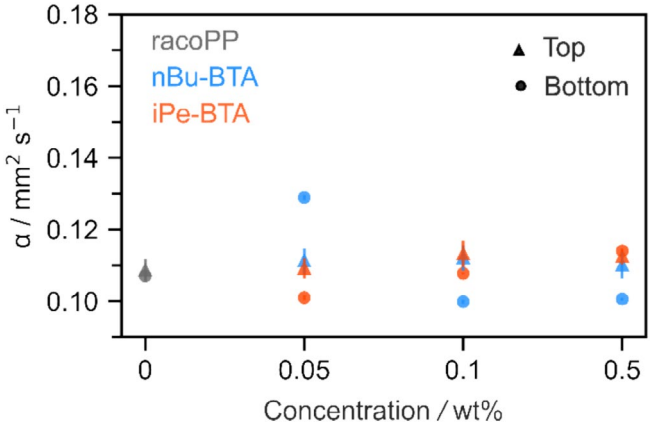

FIGURE 2 | Thermal diffusivity α of an injection-molded neat racoPP specimen and racoPP specimens with varying content of nBu-BTA and iPe-BTA, obtained by LFA. Measurements are performed on cylinders measuring 1 cm in diameter, cut from the top and bottom halves of the original injection-molded samples.

anisotropy is not solely based on the presence of BTA, but the BTA addition merely enhances the orientation of PP crystallites. Especially, the SAXS pattern obtained from the bottom position exhibits reflexes of greater intensity along the meridional direction, suggesting that the lamellar PP crystallites have grown in the perpendicular flow direction. This can be attributed to the alignment of chain segments in the direction of the flow, leading to the formation of primary nuclei. The absence of a horizontal streak indicates that these nuclei are not long fibrillar shish crystals; instead, they likely represent smaller clusters of aligned chains. Lamellar PP structures grow perpendicularly from these oriented nuclei in a secondary crystallization stage [12]. Nevertheless, this orientation of lamellar PP structures is more dominant when a nucleating agent is added to the racoPP melt. The nBu- and iPe-BTA both lead to meridional maxima, which are clearly visible for all measurement positions. The sample containing iPe-BTA leads to the most pronounced high-intensity reflexes at the bottom and middle sample positions. This observation is attributed to the superior nucleation capability of iPe-BTA compared with nBu-BTA, as evidenced by

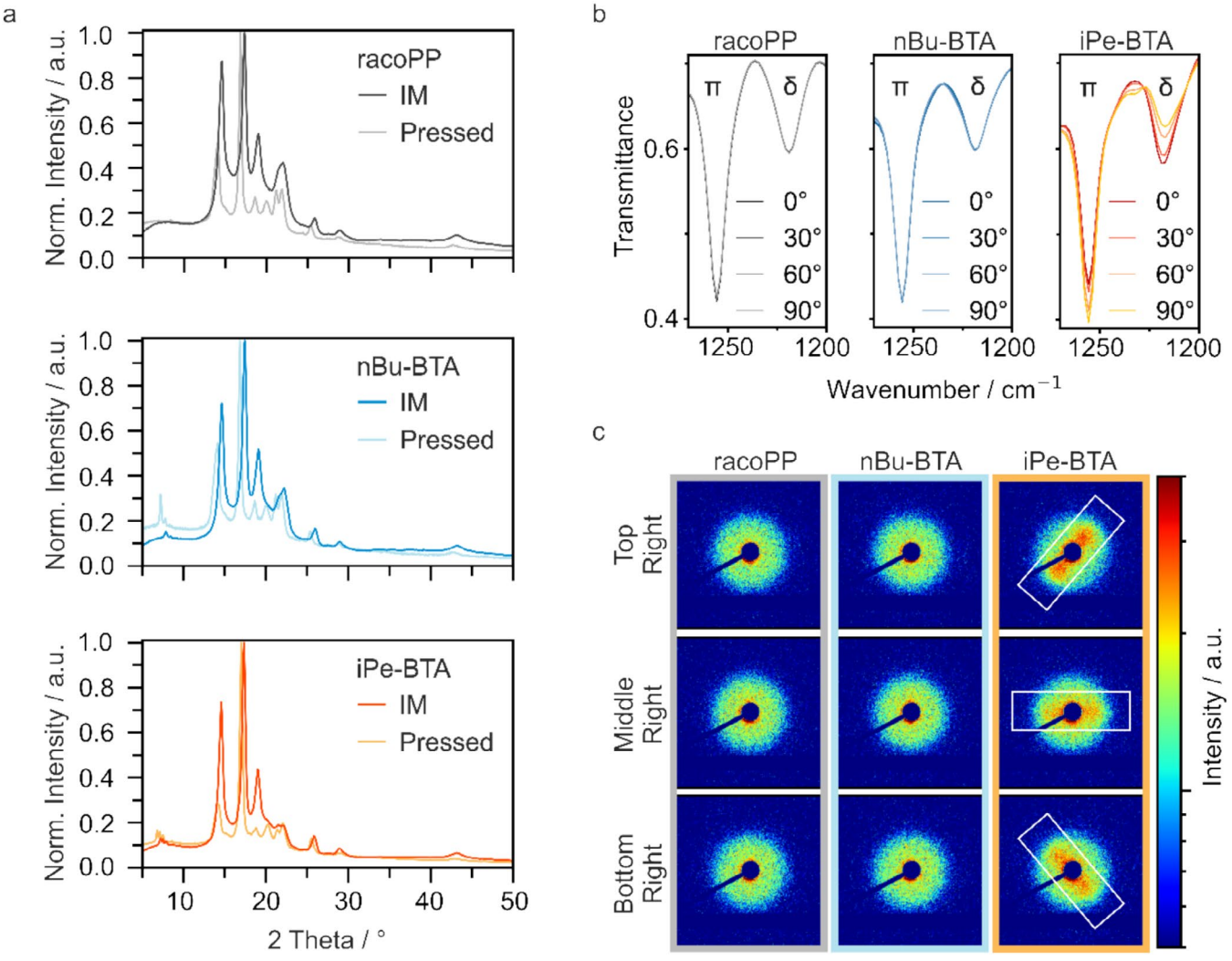

FIGURE 3 | Structural characterization of neat racoPP (gray), racoPP with 0.5 wt% nBu-BTA (blue) and racoPP with 0.5 wt% iPe-BTA (orange). (a) XRD patterns comparing the injection-molded and compression-molded samples. Intensities are normalized to the highest peaks. (b) IR spectra of the compression-molded samples at the bottom-middle position using polarized incident IR radiation. (c) 2D SAXS patterns of the compression-molded samples at the designated positions (white boxes indicating the orientation of intensity maxima).

the higher crystallization temperature of racoPP with iPe-BTA versus nBu-BTA (Figure S3). In summary, the lamellar polymer structures in injection-molded racoPP are oriented perpendicularly to the flow direction. This orientation and its extent, however, depend on the position within the sample and the addition or omission of a BTA nucleating agent.

We verified whether the structural differences between the sample positions and the sample types affect the through-plane thermal diffusivity, using light flash analysis (LFA). Figure 2 shows the obtained results for cylindrical samples with a diameter of 1 cm obtained from the top and bottom halves of each injection-molded specimen.

Comparing the values for the top and bottom of the samples, no correlation between thermal diffusivity and specimen position can be found, although SAXS determined differences in structural anisotropy. The reason for this could be that the observed structural anisotropy reflects an in-plane crystallite orientation, whereas LFA probes the through-plane thermal diffusivity of the samples perpendicular to the flow direction during injection molding. Also, there is no discernible trend in thermal diffusivity with varying BTA concentrations. This aligns with the consistency observed in the XRD measurements conducted across different BTA concentrations (Figure S2). The variations in thermal diffusivity among neat racoPP, racoPP with 0.5 wt% nBu-BTA, and racoPP with 0.5 wt% iPe-BTA are also subtle, below 0.04 $mm^2 s^{-1}$, despite the differences in crystallinity. It appears that these differences are not sufficient to induce notable changes in through-plane thermal transport. We suspect that the amorphous components predominantly govern phonon propagation and, therefore, limit thermal diffusivity, even for samples with high crystallinity [27]. All in all, through-plane thermal diffusivity of the injection-molded samples is independent of factors such as sample position, BTA concentration, or BTA type.

2.2 | Compression-Molded Samples

To obtain thin films from the injection-molded specimens, we performed compression molding at a temperature of 180°C, which is well above the melting point of racoPP. After gradually cooling the samples to 90°C under pressure, films with a thickness of approximately 0.1 mm were obtained. Infrared (IR) spectroscopy, XRD, and SAXS measurements were conducted to analyze the effect of the pressing process on the racoPP structure (Figure 3).

Figure 3a compares the XRD results before and after compression molding of the neat racoPP, racoPP with 0.5 wt% nBu-BTA, and racoPP with 0.5 wt% iPe-BTA. Due to the slower cooling rate of the pressed specimens in contrast to the injection-molded samples, all thin films exhibit an increased degree of crystallinity compared with their injection-molded counterparts. For racoPP with iPe-BTA and neat racoPP, the crystallinities increased to 57% and 54%, respectively, which can be well explained by enhanced crystal growth for slow cooling rates. The crystallinity of compression-molded racoPP with nBu-BTA lies beneath those values at 50%. In addition, the presence of an additional reflex at about 20° shows the formation of a certain fraction of the γ modification of racoPP, caused by the shear stress and low cooling rate during compression molding [28]. The persistence of the peaks below 10° for the samples containing a BTA nucleating agent verifies that the BTA crystal structures are present within these compression-molded samples.

Polarized IR spectroscopy offers insights into the orientation of the polymer chains. Since specific vibrational modes of PP are polarized, the absorption of the corresponding frequencies relies on the polarization angle of the incident radiation [29]. The full spectra of all measured samples and sample positions with light polarized by 0°, 30°, 60°, and 90° are provided in Figure S5. The IR spectra of neat racoPP and racoPP containing 0.5 wt% nBu-BTA do not show a dependency on the polarization angle of incident radiation (Figure 3b). This points towards an isotropic orientation of the PP chains in these samples. In the spectra of racoPP with 0.5 wt% iPe-BTA, slight differences can be seen when utilizing light polarizations ranging from 0° to 90°. As the polarization angle of the incident light decreases, the absorption of parallel-polarized frequencies (π) increases, whereas the absorption of perpendicular-polarized frequencies (δ) decreases. Although these changes are subtle, the example bands in Figure 3b, corresponding to the perpendicular-polarized mode at 1218 cm^{-1} and the parallel-polarized mode at 1256 cm^{-1}, demonstrate the dependence on incident light polarization [29]. Similar observations are noted across the other sample positions of racoPP containing 0.5 wt% iPe-BTA. This result indicates that the presence of iPe-BTA leads to a weak but observable preference for the orientation of the PP chains and thus of the lamellar crystallites. IR spectroscopy is supplemented by 2D SAXS at 11 measurement positions per sample, evenly distributed to cover the top, center, and bottom of the specimen. In Figure 3c, a representative selection of three measurement points taken from the right-hand side of each sample is shown (top-right, middle-right, bottom-right). Details on the locations of the measurement points and the SAXS patterns for all sample positions are provided inFigures S6 and S7. The 2D SAXS data corresponding to neat racoPP and racoPP with nBu-BTA show consistent intensity maxima across the entire azimuthal angle range, resulting in a circular SAXS pattern. This demonstrates an isotropic distribution of the lamellar crystallites, which is consistent with the isotropic orientation of the PP chains revealed by IR spectroscopy. Although the PP chains are aligned within the individual crystallites, the crystallites themselves are small relative to the area analyzed by IR spectroscopy and are oriented randomly. This results in an overall appearance of isotropic PP chain orientation when examined using IR spectroscopy. As discussed, the XRD data show crystalline nBu-BTA after pressing the samples. However, the preferential spatial orientation of the PP crystallites was lost during the compression-molding step. Several possible reasons must be considered: Either the nBu-BTA assemblies are not aligned during compression molding, or the nBu-BTA assemblies are oriented, but the supramolecular additive does not dominate the nucleation process. Looking at the iPe-BTA, we may gain some clues on the most relevant contribution to this loss of orientation. The measurements conducted on racoPP with 0.5 wt% iPe-BTA reveal broad meridional maxima, being distinctly different from the neat racoPP and the case of nBu-BTA. These results are consistent with the IR spectroscopic data. Considering the similarity between nBu-BTA and iPe-BTA in inducing crystallite orientation within the injection-molded samples, no difference in the orientation of the supramolecular

assemblies consisting of nBu-BTA or iPe-BTA is expected in the compression-molded specimens. However, the cooling kinetics is much slower in this case, allowing for significant differences in the nucleation and growth mechanism of racoPP. Since nBu-BTA is a less effective nucleating agent for PP and shear is absent during polymer crystallization, we suspect that the intrinsic self-nucleation of racoPP plays a dominant role [20, 21]. This leads to randomly oriented crystallites and competes with the nBu-BTA nucleation sites, leading to an isotropic SAXS pattern.

The orientations of the dumbbell-like maxima determined for racoPP with 0.5 wt% iPe-BTA are highlighted by white rectangles (Figure 3c). They are all oriented perpendicularly to the sample edge, indicating a respective coplanar orientation of the PP lamellae. This result is attributed to the outward flow of the PP melt during the pressing process. The flow profile orients the BTA fibrils outwards to the center. As the lamellae grow perpendicularly to the BTA nuclei, they result in a coplanar arrangement with respect to the sample edge, which we observe in the SAXS patterns.

The low thickness of the samples allows measuring the in-plane thermal diffusivities using lock-in thermography (LIT). This technique is based on periodic heating of the thin film using a focused point laser, while the temperature distribution is monitored with an IR camera. Fourier Transformation is applied, and the obtained amplitude and phase data are linearized relative to the distance from the center of the heat source. The thermal diffusivity is then calculated using the so-called slope method [30, 31]. The compression-molded racoPP films without BTA, with 0.5 wt% nBu-BTA, and with 0.5 wt% iPe-BTA are measured in the bottom third, middle third, and top third of the samples. All measurements yield an isotropic amplitude and phase signal, as exemplified by the bottom segment of the racoPP sample containing 0.5 wt% iPe-BTA (Figure 4a). This shows that the preferential orientation of lamellar structures, as confirmed by 2D SAXS, does not result in anisotropic thermal transport. Amorphous regions between the crystalline PP lamellae act as a bottleneck for thermal transport [27]. Apparently, even for high crystallinities, amorphous regions persist in all directions and uniformly limit phonon propagation. Within the boundaries of the processing parameters explored in this study, processing racoPP with or without a nucleating agent does not result in anisotropic heat transport.

In Figure 4b the obtained thermal diffusivity values are presented. Given that structural anisotropy does not dictate a preferred direction for heat transport, it is unsurprising that the diffusivity remains consistent across different sample positions. Slightly elevated values are observed in the sample containing 0.5 wt% iPe-BTA compared to those with nBu-BTA or neat racoPP. However, the difference is too marginal to be deemed significant. Overall, a consistent thermal diffusivity is apparent across variations in nucleating agent and sample position.

Careful consideration is needed when comparing the through-plane thermal diffusivity obtained by LFA with the in-plane thermal diffusivity measured via LIT, as these methods are inherently based on different measurement principles. Despite the limitations of LFA to the thick injection-molded specimens and LIT to thin films, the ability to measure both provides valuable insights. It is notable that the thermal diffusivity of the injection-molded samples is slightly lower than the thermal diffusivity of the pressed samples. This may be attributed to the higher crystallinity of the compression molded (50%–57%) compared with the injection-molded samples (38%–46%), but may also be reasoned by the inherent differences of the measurement techniques. More importantly, it is evident that the results of all performed thermal diffusivity measurements lay within the small range of 0.10–0.15 $mm^2 s^{-1}$. Taking the heat capacity and density of racoPP into account, this leads to thermal conduction values between 0.15 and 0.22 $W (m K)^{-1}$, regardless of the processing or the addition of BTA. Furthermore, the structural anisotropy, driven by the in-plane orientation preference of the PP lamellae, is not reflected in either the through-plane or in-plane thermal transport direction. This can be attributed to the amorphous regions, which uniformly limit the phonon propagation and, therefore, function as bottlenecks for thermal transport [27]. For industrial applications of racoPP, this resilience of thermal transport represents a practical advantage. Whether the material is injection-molded, pressed into thin films, or whether BTAs are added to alter optical and mechanical properties, there is no need to be concerned about a preferred direction of heat

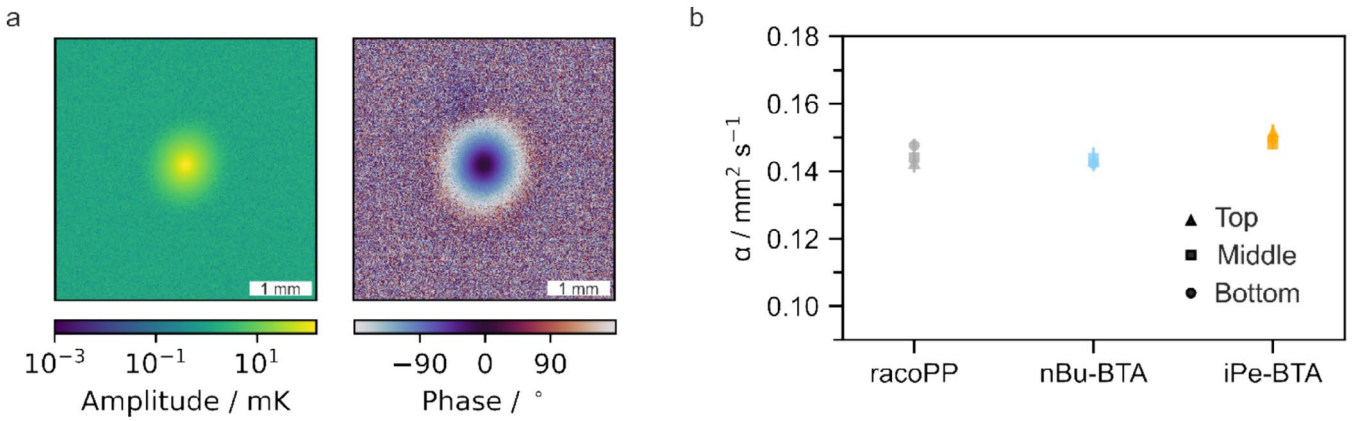

FIGURE 4 | LIT of compression-molded samples with a thickness of 0.1 mm. (a) Amplitude and phase signal obtained for compression-molded racoPP containing 0.5 wt% iPe-BTA. (b) Thermal diffusivity α of an injection-molded neat racoPP specimen and racoPP specimens with 0.5 wt% nBu-BTA and 0.5 wt% iPe-BTA. Five locations on each sample part (top, middle, and bottom) were probed.

transport or significant changes in the magnitude of thermal conduction.

3 | Conclusion

The impact of BTA additives on the thermal diffusivity of racoPP was assessed. Hereby, neat racoPP was compared with racoPP containing the efficient nucleating agent iPe-BTA and racoPP containing the less efficient nucleating agent nBu-BTA. The specimens were additionally classified into injection-molded and compression-molded samples to analyze potential processing effects. Structural information was obtained using XRD, SAXS, and IR spectroscopy. The results demonstrate that the crystal structure of racoPP is notably influenced by both processing method and the presence of BTAs. Differences in crystallinity and orientation of the PP lamellae were determined. On the contrary, the thermal diffusivity of racoPP exhibits remarkable resilience to such changes. Although it limits the ability to easily tune thermal transport, it also ensures the consistent performance that is often required in industrial applications.

4 | Experimental

4.1 | Sample Preparations

N,N′,N″-tris(3-methylbutyl)benzene-1,3,5-tricarboxamide (iPe-BTA) and N,N′,N″-tris(n-butyl) benzene-1,3,5-tricarboxamide (nBu-BTA) were synthesized and characterized as described previously [32]. *RD208CF* (Borealis AG), a random polypropylene copolymer (racoPP), was obtained as a fine powder and used as received. Two powder masterbatches containing 2 wt% of the supramolecular additives were prepared by carefully mixing 23.52 g of the racoPP with 0.48 g of the respective additive in a mortar.

Compounding was carried out at 230°C with a corotating twin-screw microcompounder (*Xplore 15 mL*, [*DSM*]) under nitrogen atmosphere at a residence time of 5 min and a rotational speed of 40 rpm. Three different concentrations of each of the supramolecular additives in racoPP (0.5, 0.1, and 0.05 wt.%) were achieved by a dilution series. In the first step of this dilution series, 12.5 g of a master batch with a concentration of 2.0 wt.% of the additive was compounded until a homogeneous polymer melt was obtained. After discharging the polymer melt, approximately 4.49 g of the molten polymer-additive mixture remained in the compounder, which was then diluted to the selected concentration by adding a corresponding amount of neat racoPP.

Injection molding was carried out using a microinjection-molding machine, *Xplore 12 mL* (*DSM*). The barrel temperature of the injection-molding unit was set to 230°C. The homogeneous polymer melt was transferred from the compounder to the microinjection-molding machine and then injected into a polished mold at an injection pressure of 6 bar for the duration of 20 s, resulting in round-shaped platelets with a diameter of 27 mm and a thickness of 1.1 mm. For each polymer-additive concentration, about five round specimens were obtained. Several neat racoPP round specimens were produced in the same way and used as references.

For the thin film preparation, we selected injection-molded racoPP specimens with additive concentrations of 0.05 wt%, 0.1 wt%, and 0.5 wt% and a neat racoPP specimen as a reference. To produce homogeneous thin films, an injection-molded platelet was placed in the center of a Teflon spacer with a diameter of 90 mm and a thickness of 0.1 mm and sandwiched between two Kapton foils. The sandwich was placed in a two-column lab press (*PW 20 H HKP300-ø165*, *PO Weber GmbH*) at 180°C and loaded with a force of 2.5 kN for 3 min. The force was then increased to 15 kN, and the press was slowly cooled to 90°C within approximately 35 min before the thin sample was removed from the press. The resulting samples have a diameter of 89.5 mm and a thickness of 0.1 mm.

4.2 | Characterization by XRD, SAXS, IR Spectroscopy, Differential Scanning Calorimetry, and Helium Pycnometer

XRD was performed via a Bragg–Brentano geometry *Empyrean* diffractometer by *Malvern Panalytical BV* in spinning mode. It is equipped with a pixel detector using a copper K_α ($\lambda = 1.54$ Å) radiation source. The instrument provides the software *Pananlytical's Highscore Plus* for data analysis. The crystallinity of the processed racoPP samples was estimated by integrating the relative intensities of the Bragg reflections and amorphous halos [33]. Examples are given in Figure S1.

SAXS measurements were performed on a lab-based *Double Ganesha AIR* system by *SAXSLAB/Xenocs*. This system is equipped with a copper rotating anode (*MicroMax 007HF* by *Rigaku Corporation* $\lambda = 1.54$ Å) and position-sensitive *Pilatus* detectors from *Dectris Ltd* (300 K for SAXS).

Polarized broadband IR spectroscopy was applied with a *Vertex 70* by *Bruker Corporation* in combination with a corresponding polarizer.

DSC measurements were performed on a *Discovery DSC 2500* by *TA Instruments Inc*. The heat capacity of racoPP was determined to be 1.819 ± 0.004 J $(\mathrm{gK})^{-1}$. It was calculated from three measurements, all according to the American Society for Testing and Materials (ASTM) E1269 standard. The crystallization peak temperatures of racoPP were determined during cooling at a rate of 20°C/min, under nitrogen, after holding at 230°C for 15 min.

To determine the density of racoPP, a small amount of the injection-molded sample was measured with an *Ultrapyc 1200e* helium pycnometer by *Quantachrome Instruments*. The average density was calculated to be $0.815 \pm 0.003\,\mathrm{g\,cm^{-3}}$ using 25 individual measurement results.

4.3 | Lock-In Thermography

Each compression-molded sample was coated with a thin layer of carbon (10–20 nm) on both sides. They were excited periodically with a frequency of 1.3 Hz using a point laser (*51nano-N520-0.9-O05-P-12-4-28-0-150*) by *Schäfter + Kirchhoff GmbH* with a power of 0.9 mW. The temperature evolution was monitored with an *ImageIR 9430* research IR camera *by InfraTec*

GmbH, with a spectral window ranging from 1.5 to 5.5 μm. It was mounted with an $M = 1.0\times$ microscopy objective. The experiments were performed in a vacuum chamber ($p \leq 0.02$ mbar) containing an optically transparent N-BK7 glass window to minimize convective heat losses. The time–temperature data were converted by Fourier transformation to an amplitude and phase signal via the *IRBIS* software provided by *InfraTec GmbH*. The linearized amplitude and phase signals as a function of the distance from the excitation point of the laser were then used to obtain the thermal diffusivity (slope method).

Acknowledgments

We thankfully acknowledge the support of the Collaborative Research Centre 1585, Projects A04 and C05 of the German Research Foundation (grant number: 492723217). We acknowledge support from the Keylabs "Mesoscale Characterization" and "Small Scale Polymer Processing" of the Bavarian Polymer Institute (BPI). This research benefited from SAXS instrumentation funded by Deutsche Forschungsgemeinschaft (grant number INST 91/38-41).

Conflicts of Interest

The authors declare no conflicts of interest.

References

1. H. A. Maddah, "Polypropylene as a Promising Plastic: A Review," *American Journal of Polymer Science* 6 (2016): 1–11.

2. S. Radhakrishnan and P. S. Sonawane, "Role of Heat Transfer and Thermal Conductivity in the Crystallization Behavior of Polypropylene-Containing Additives: A Phenomenological Model," *Journal of Applied Polymer Science* 89 (2003): 2994–2999.

3. M. Gahleitner, C. Grein, S. Kheirandish, and J. Wolfschwenger, "Nucleation of Polypropylene Homo- and Copolymers," *International Polymer Processing* 26 (2011): 2–20.

4. P. M. Kristiansen, A. Gress, P. Smith, D. Hanft, and H.-W. Schmidt, "Phase Behavior, Nucleation and Optical Properties of the Binary System Isotactic Polypropylene/N,N′,N″-Tris-Isopentyl-1,3,5-Benzene-Tricarboxamide," *Polymer* 47 (2006): 249–253.

5. N. Mohmeyer, B. Müller, N. Behrendt, et al., "Nucleation of Isotactic Polypropylene by Triphenylamine-Based Trisamide Derivatives and Their Influence on Charge-Storage Properties," *Polymer* 45 (2004): 6655–6663.

6. Y.-F. Zhang, H. Chen, B.-B. Liu, Y.-H. Gu, and X.-X. Li, "Isothermal and Non-Isothermal Crystallization of Isotactic Polypropylene Nucleated With 1,3,5-Benzenetricarboxylic Acid Tris(Cyclohexylamide)," *Thermochimica Acta* 590 (2014): 226–231, https://doi.org/10.1016/j.tca.2014.07.007.

7. Y.-f. Zhang and H. Chen, "Effects of Nucleating Agent 1,3,5-Benzenetricarboxylic Acid Tris(Cyclohexylamide) on Properties and Crystallization Behaviors of Isotactic Polypropylene," *Colloid and Polymer Science* 292 (2013): 493–498.

8. A. A. Abreu, S. I. Talabi, and A. de Almeida Lucas, "Influence of Nucleating Agents on Morphology and Properties of Injection-Molded Polypropylene," *Polymer Advances in Technology* 32 (2021): 2197–2206.

9. Z. Horváth, A. Menyhárd, P. Doshev, et al., "Improvement of the Impact Strength of Ethylene-Propylene Random Copolymers by Nucleation," *Journal of Applied Polymer Science* 133 (2016): 43823.

10. R. Pantani, I. Coccorullo, V. Speranza, and G. Titomanlio, "Modeling of Morphology Evolution in the Injection Molding Process of Thermoplastic Polymers," *Progress in Polymer Science* 30 (2005): 1185–1222.

11. B. Yang, J.-Z. Lin, R. Xia, et al., "Correlation Between Solidification Behavior and Melt Crystallization Kinetics of IsotacticPolypropylene (iPP) During Injection Molding," *Journal of Macromolecular Science, Part B* 53 (2014): 462–473.

12. R. H. Somani, B. S. Hsiao, A. Nogales, et al., "Structure Development During Shear Flow-Induced Crystallization of i-PP: In-Situ Small-Angle X-Ray Scattering Study," *Macromolecules* 33 (2000): 9385–9394.

13. M. Kandemir, İ. Karagöz, and H. Sepetcioglu, "Experimental Investigation of Effects of the Nucleating Agent on Mechanical and Crystallization Behavior of Injection-Molded Isotactic Polypropylene," *El-Cezeri Fen Ve Mühendislik Dergisi* 10 (2022): 110–120.

14. R. Čermák, M. Obadal, P. Ponížil, M. Polášková, K. Stoklasa, and A. Lengálová, "Injection-Moulded α- and β-Polypropylenes: I. Structure vs. Processing Parameters," *European Polymer Journal* 41 (2005): 1838–1845.

15. G. Kalay and M. J. Bevis, "Processing and Physical Property Relationships in Injection-Molded Isotactic Polypropylene. 1. Mechanical Properties," *Journal of Polymer Science. Part B, Polymer Physics* 35 (1997): 241–263.

16. B. Purgleitner, D. Viljoen, I. Kühnert, and C. Burgstaller, "Influence of Injection Molding Parameters, Melt Flow Rate, and Reinforcing Material on the Weld-Line Characteristics of Polypropylene," *Polymer Engineering and Science* 63 (2023): 1551–1566.

17. D. R. Fitchmun and Z. Mencik, "Morphology of Injection-Molded Polypropylene," *Journal of Polymer Science: Polymer Physics Edition* 11, no. 5 (2003): 951–971, https://doi.org/10.1002/pol.1973.180110512.

18. F. Liu, C. Guo, X. Wu, X. Qian, H. Liu, and J. Zhang, "Morphological Comparison of Isotactic Polypropylene Parts Prepared by Micro-Injection Molding and Conventional Injection Molding," *Polymer Advances in Technology* 23 (2011): 686–694.

19. D. Libster, A. Aserin, and N. Garti, "Advanced Nucleating Agents for Polypropylene," *Polymers for Advanced Technologies* 18 (2007): 685–695.

20. M. Blomenhofer, S. Ganzleben, D. Hanft, et al., "'Designer' Nucleating Agents for Polypropylene," *Macromolecules* 38 (2005): 3688–3695.

21. J. Wang, Q. Dou, X. Chen, and D. Li, "Crystal Structure and Morphologies of Polypropylene Homopolymer and Propylene-Ethylene Random Copolymer: Effect of the Substituted 1,3,5-Benzenetrisamides," *Journal of Polymer Science. Part B, Polymer Physics* 46 (2008): 1067–1078.

22. F. Abraham, S. Ganzleben, D. Hanft, P. Smith, and H. W. Schmidt, "Synthesis and Structure–Efficiency Relations of 1,3,5-Benzenetrisamides as Nucleating Agents and Clarifiers for Isotactic Poly(Propylene)," *Macromolecular Chemistry and Physics* 211 (2010): 171–181.

23. Y.-F. Zhang, P.-Z. Zhou, Y.-Z. Jiang, and X. Yang, "The Relationship Between Side Chain Isomerism of Aliphatic C4 Substituted 1,3,5-Benzenetricarboxylamides and Nucleation Effects in Isotactic Polypropylene," *Thermochimica Acta* 655 (2017): 219–225.

24. T. Bárány and J. Karger-Kocsis, *Polypropylene Handbook: Morphology, Blends and Composites* (Springer International Publishing, 2019).

25. P. M. Kristiansen, "PhD Thesis," (2004), Eidgenössische Technische Hochschule (ETH), Zürich.

26. J. C. Wittmann and B. Lotz, "Epitaxial Crystallization of Polymers on Organic and Polymeric Substrates," *Progress in Polymer Science* 15 (1990): 909–948.

27. K. Herrmann, S. Freund, F. Eller, et al., "Microstructural and Thermal Transport Properties of Regioregular Poly(3-Hexylthiophene-2,5-Diyl) Thin Films," *Materials* 15 (2022): 7700.

28. Y. Wang, J. Zhao, M. Qu, et al., "An Unusual Promotion of γ-Crystals in Metallocene-Made Isotactic Polypropylene From Orientational Relaxation and Favorable Temperature Window Induced by Shear," *Polymer* 134 (2018): 196–203.

29. S. Krimm, *Fortschritte der Hochpolymeren-Forschung* (Springer, 1960), 51–172.

30. A. Salazar, A. Mendioroz, and R. Fuente, "The Strong Influence of Heat Losses on the Accurate Measurement of Thermal Diffusivity Using Lock-In Thermography," *Applied Physics Letters* 95 (2009): 121905.

31. A. Salazar, A. Mendioroz, R. Fuente, and R. Celorrio, "Accurate Measurements of the Thermal Diffusivity of Thin Filaments by Lock-In Thermography," *Journal of Applied Physics* 107 (2010): 043508.

32. A. Timme, R. Kress, R. Q. Albuquerque, and H. W. Schmidt, "Phase Behavior and Mesophase Structures of 1,3,5-Benzene- and 1,3,5-Cycl ohexanetricarboxamides: Towards an Understanding of the Losing Order at the Transition Into the Isotropic Phase," *Chemistry* 18 (2012): 8329–8339.

33. G. W. Becker, *Kunststoff-Handbuch. 3, Technische Thermoplaste: 4. Polyamide* (Hanser, 1998).

Supporting Information

Additional supporting information can be found online in the Supporting Information section.